NANOMATERIALS SCIENCE & ENGINEERING
Vol. 4, No. 1, pp. 27-37 (2022)

RESEARCH ARTICLE

https://doi.org/10.34624/nmse.v4i1.29374

Conductivity and transmittance enhancement of PEDOT:PSS thin films by graphene addition

Felipe Teixeira Mabilia*, Shu Hui Wang

University of São Paulo, Polytechnic School, Department of Metallurgical and Materials Engineering, Av. Professor Mello Moraes, 2463, CEP: 05508-030, São Paulo/SP, Brazil
**Corresponding author, e-mail address: felipe.mabilia@usp.br*

Received 17 June 2022; accepted 16 November 2022; published online 20 December 2022

ABSTRACT

Compared to conventional inorganic semiconductors, organic semiconductors present several advantages, such as cost-effectiveness, mechanical toughness, synthesis versatility and simple production set-ups, among others. In this work, we have prepared conductive solid films based on multilayer graphene (mG) and poly(3,4-ethylenedioxythiophene):polystyrenesulfonate (PEDOT:PSS) from liquid dispersions. mG-10.6 wt% dispersion in isopropanol was prepared in two steps. In the first step, graphite was submitted to liquid phase exfoliation in N-methyl-pyrrolidone (NMP) (5.3 wt% of mG), then, in the following step, NMP was removed by precipitation and mG redispersed, using polyethyleneimine and acetic acid-1M in isopropanol, respectively. The nanocomposite films were prepared from dispersions of mG and PEDOT:PSS, by spin-coating, to reach pre-established solid concentrations of 10.2 wt% and 49.9 wt% of mG. The optical and electrical properties of the thin films were characterized using UV-Visible Spectroscopy and an adapted four-probe resistance measurement, while Raman Spectroscopy, Scanning Electron Microscopy (SEM), and Atomic Force Microscopy (AFM) were applied to analyze their morphological features. The thin films showed high transmittances, even multilayer, upholding more than 85% for three-layer films, similar to that found in the single-layer ones. The sheet resistances of the films were detected in the range of a few hundreds of Ω/□. Both transmittance and sheet resistance of the films were improved when compared to those found in pristine mG and pristine PEDOT:PSS, which is due to higher charge mobility in the nanocomposite. Raman Spectroscopy showed the formation of the composite by π-π interaction and the conformational change in the polymer chains was confirmed by peak shift. SEM analysis showed that the films are largely homogeneous, and mG is uniformly dispersed, nevertheless the mG platelets appear to be standing up from the film (AFM). The phase image (AFM) allows the differentiation between rigid and soft regions, i.e., mG/PEDOT and PSS, respectively. Semiconductive nanocomposites having high load of mG were successfully prepared, and their resulting electrical and optical properties make them suitable to be used, e.g., as transparent electrodes, in the fabrication of displays, lighting devices and photovoltaic materials or as multipurpose conductive inks.

1. INTRODUCTION

Conductive transparent electrodes (TCEs) have high electrical conductivity, low sheet resistance and transparency to visible light [1,2], essential characteristics for organic solar cells (OPVs), displays, organic light-emitting diodes (OLEDs), liquid crystal displays, touch displays, lasers [3] and electrochromic devices [4], among other applications. The most common material used in the production of TCEs is indium tin oxide (ITO), however alternative materials have been investigated to replace ITO due to the high cost and scarcity of indium. Additionally, ITO thin films are fragile, making them difficult to be used in the manufacture of flexible devices, do not adhere well to polymeric materials, require high temperatures and high vacuum for their manufacture, and have low chemical resistance to acidic and alkaline environments [1-8].

Metallic nanowires, carbon nanotubes, graphene and conductive polymers have been

suggested as possible replacements for ITO [1-7]. Poly(3,4-ethylenedioxythiophene):poly(styrene-sulfonate) (PEDOT:PSS) is a polymer blend commercially available as aqueous dispersion which is solution processable and forms a highly flexible, light-transparent, thermally stable film, commonly used as a transparent hole transport layer in OLEDs and OPVs [2,4]. However, PEDOT:PSS thin films require improvements in conductivity to be viable in certain applications as TCE [7]. Due to its low cost and easiness to form thin films with excellent properties, there is a great academic and technological interest in increasing its conductivity. Modifications were carried out, such as the addition of organic solvents to the dispersion before the deposition of the films [4,7,9,10], treatments of formed films [1,3,5,7] with solvents or acids or even incorporation of conductive nanoparticles, forming nanocomposites, among which composites with graphene [11], graphene oxide [12], graphene quantum dots [13], and carbon nanotubes [2] stand out.

Graphene is a material composed of carbon atoms arranged in a two-dimensional structure in a honeycomb lattice [14-16]. The conjugation of π bonds results in excellent electrical properties, making graphene an interesting option for the production of electronic devices, even as an additive in composites [14]. In addition, graphene presents high electronic mobility, high transparency, flexibility and stability, qualifying it for electronic applications [17]. On the other hand, the difficulty of producing quality graphene on a large scale is a disadvantage for the use of this material. Mechanical exfoliation of graphite produces the best samples, but it is not easily scalable. Liquid-phase exfoliation of graphite is an inexpensive and scalable production method of graphene, which consists of adding graphite to solvents such as N-methylpyrrolidone (NMP), isopropyl alcohol (IPA) or dimethylformamide (DMF) and dispersing the graphene sheets with the aid of sonication [18,19].

Exfoliated graphenes in composites with PEDOT:PSS [11] increased the conductivity from 0.16 S/cm to 60 S/cm for 0.47% by weight of graphene, with transmittances above 90% [11]. Hong et al. [20] produced PEDOT:PSS/graphene composites from an aqueous dispersion of graphene and used the resulting composite films as counter electrodes for dye-sensitized solar cells. The transmittance was over 80% and the energy conversion efficiency was 4.5% under white light at 100 mW AM 1.5 [20]. Hilal and Han [21] obtained graphene dispersed in NMP after a series of steps and produced composite films of PEDOT:PSS/graphene with different concentrations of the nanomaterial, obtaining sheet resistances lower than 10 Ω/□ and transmittances above 70% when deposited on ITO/glass [21]. Park et al. [22] produced hybrid PEDOT:PSS/graphene films by depositing PEDOT:PSS films on graphene films, obtaining sheet resistances of about 100 Ω/□ and transmittances above 80% [22].

In this work multilayer graphene produced by exfoliation in NMP (mG_NMP) was used to prepare PEDOT:PSS/mG composite films, which were characterized by Raman Spectroscopy, UV-Visible Spectroscopy, Scanning Electron Microscopy (SEM), Atomic Force Microscopy (AFM) and electrical conductivity measurements. The results have shown their potential application as TCEs and conductive inks.

2. MATERIALS AND METHODS

2.1. Powder Synthesis

Table 1. Compositions of the mG and PEDOT:PSS/mG dispersions.

Dispersion	mG_NMP mL	PEI mL	HAc_IPA 1 M mL	D2 µL	PEDOT/PSS µL	DMSO µL	Solids mg/mL	PEI wt%	mG wt%	PEDOT/PSS wt%
D1	10	1.1	5	-	-	-	10.7	2.1	97.9	-
D2	10	0.42	5	-	-	-	10.6	0.8	99.2	-
D3	-	-	-	420	400	100	9.6	0.4	49.9	49.3
D4	-	-	-	95	800	200	9.0	0.08	10.2	89.7
DP	-	-	-	-	1600	400	8.8	-	-	100
DP*	-	-	0.16	-	1600	400	8.8	-	-	100

Table 2. Film deposition parameters.

Film	Dispersion	Speed	Time (s)	Layers
1	D1	200	20-60	1
2	D2	500	20-50	1;3
3	D3	500	30	1
4	D3	1000	30	1
5	D4	1000	30	1;3
6	D4	500	30	2
7	DP	500-1000	20-30	1
8	DP*	500-1000	20-60	1

The initial graphene dispersion (mG_NMP) was prepared from the heat treatment of graphite (Nacional de Grafite), followed by exfoliation in NMP aided by an ultrasonic bath [23]. After 220 hours in the ultrasonic bath (Quimis, model Q335D), the dispersion was centrifuged and filtered to separate the undispersed fraction. The concentration of graphene present in the dispersion determined by gravimetry was 5.25 ± 0.35 mg/mL.

Two dispersions of graphene (D1 and D2) in isopropanol (IPA) (Table 1) and two dispersions of PEDOT:PSS/mG (D3 and D4) in IPA (Table 1) were prepared.

Graphene dispersions in IPA were prepared from mG_NMP using a solution of polyethyleneimine in IPA (PEI, 1 mg/ml). D1 was prepared by adding 1.1 mL of PEI in IPA (1 mg/mL) to 10 mL of mG_NMP, followed by centrifugation, washing the precipitate with distilled water, and centrifugation again, the process was repeated three times. The precipitate was redispersed in 5 mL of HAc in IPA (1 M) and portions of 10 µL of HAc were added until mG is completely dispersed. The D2 dispersion was prepared using a similar procedure, but the quantities of the components were changed, as shown in Table 1.

D3 and D4 were prepared from D2 and PEDOT:PSS (Sigma Aldrich, code 483095). For D3, 0.4 mL of PEDOT:PSS was added to 0.42 ml of D2, followed by 0.1 ml of DMSO. D5 followed the same procedure, changing the volumes to 0.095 mL of D2, 0.8 mL of PEDOT:PSS and 0.2 mL of DMSO (Table 1). DP is a graphene-free PEDOT:PSS dispersion prepared by mixing 1.6 mL of PEDOT:PSS with 0.4 mL of DMSO in an ultrasound bath. DP* is analogous to DP, but has received HAc in IPA to aid surface wetting.

All dispersions were kept for one hour in the ultrasonic bath before film deposition to avoid the presence of possible aggregates. The dispersions were deposited on glass substrates previously cleaned with a glass cleaner (Aquabrilho®, Adespec, Brazil). This procedure aimed to increase the adhesion of the films to the substrate without the need to go through all the steps using detergent, acetone and IPA, usual in traditional glass cleaning. The depositions were carried out in a spin coater (Swin 4", model EC4 SYN 3S102-0902). The dispersion volume used was 70 µL, except for DP and DP* dispersions, for which the volume varied between 70 µL and 160 µL. Annealing was performed on a heating plate (Yotec, model YS-200S) at 120 °C during 20 minutes. The parameters used in the deposition are summarized in Table 2.

A dried thin film deposited on a glass slide was used for the characterization of mG_NMP by Raman spectroscopy, according to a previous work [24]. To evaluate the graphene after redispersion in IPA with the addition of PEI and HAc, as well as the composites and the interaction between graphene and PEDOT:PSS, Raman spectroscopy was performed using the WITec Confocal Raman Microscope (Alpha 300R model) with 532 nm (green) laser and maximum power of 45 mW. Due to the nature of the samples, it was chosen to use a lower power, of only 8 mW, to avoid any alteration in the analyzed materials.

The electrical resistance of the films was measured using a method similar to the four-probe method, but with a device with flat contacts to avoid damaging the films. A Keithley 2400 multimeter

was used to measure electrical resistance, which was used to calculate the sheet resistance of the films. The reported values refer to the average of 9 measurements.

A scanning electron microscope (FEI, Inspect F50) was used to analyze the solid films of D2 on a glass substrate and D4 on silicon (0.1 mL, 500 rpm) and mica. A thin layer of gold was deposited on the samples with glass and mica substrate before analysis.

Transmittance was measured using a UV-Vis Spectrophotometer (Cary 50 Conc). Part of the film was removed from the sample and the region was used as reference (blank). The wavelength range was from 300 nm to 800 nm. Transmittance values refer to measurements collected at 550 nm.

Atomic force microscopy (Multimode 8, Bruker) was performed in tapping mode. Films from D2 (AFM1), D3 (AFM3) and D4 (AFM2 and AFM4) were analyzed. Samples AFM1 and AFM4 are 3-layer film, while AFM2 is monolayer and sample AFM3, 2-layer. To measure the thickness of the samples, a small portion of the films was removed to create a step with the aid of a wooden toothpick.

3. RESULTS AND DISCUSSION

3.1. Raman Spectroscopy

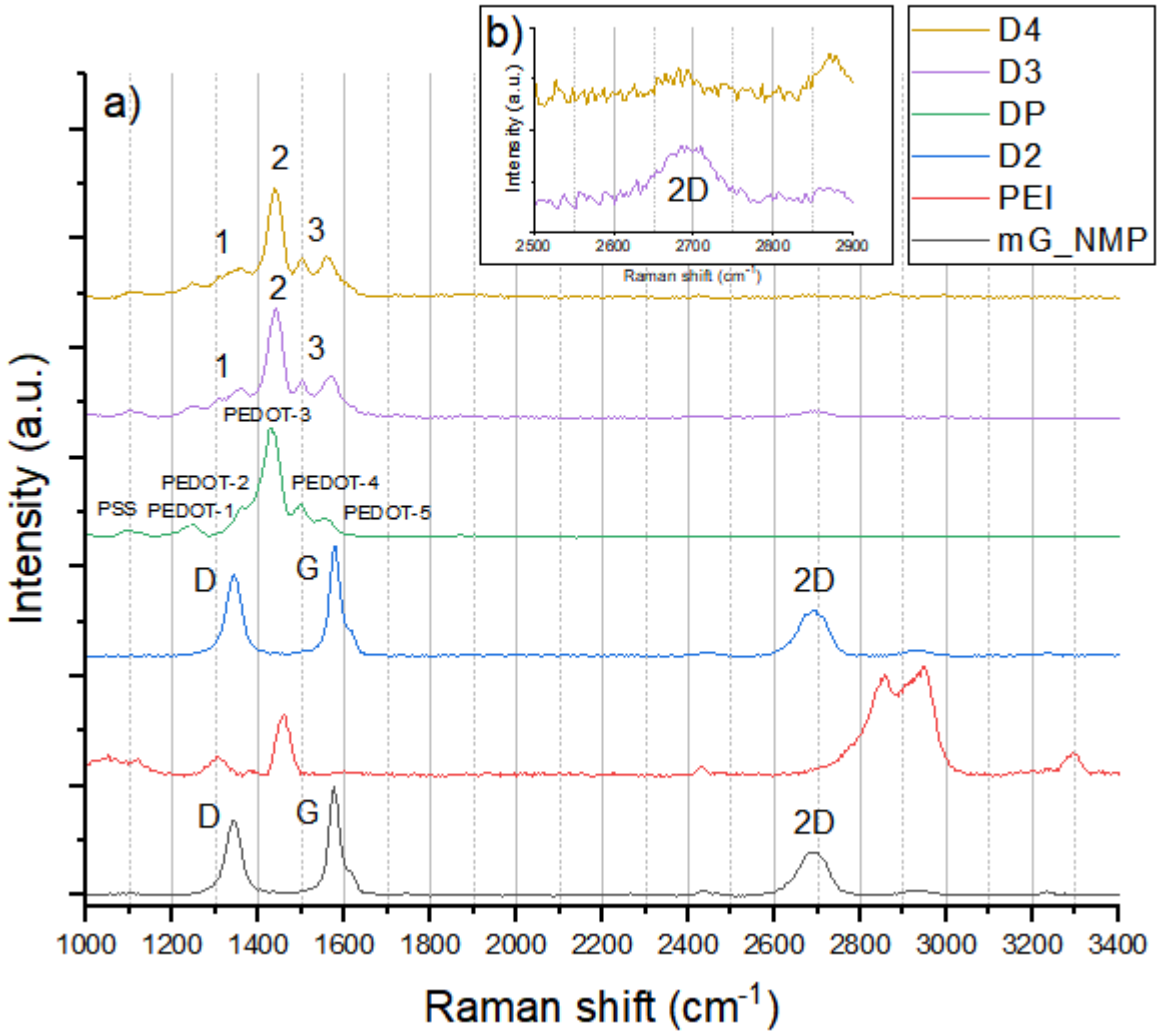

Figure 1. Raman spectra of a) mG, DP, PEI, D2, D3 and D4 and b) D3 and D4 in the 2D region (2500 cm^{-1} - 2900 cm^{-1}) magnified ~13x.

Films containing mG were characterized by Raman spectroscopy according to a previous work [24], and the position of the peaks, the ratios between the intensities of the D and G peaks (I_D/I_G) and 2D and G (I_{2D}/I_G) were determined and analyzed. The results allowed us to conclude that the graphenes present in the original mG_NMP dispersion have two to five layers. The D peak is present due to sp^2-carbon atoms at the edge of the graphene sheets, in arm-chair configuration [25], which is activated by the presence of defects [26]. The G peak results from the stretching of C-C bonds in the hexagonal basal plane. The 2D band comes from the second order vibration of D phonons [27].

Note that the mG_NMP and D2 spectra are practically identical, despite the small peak shifts, indicating that the redispersion in IPA with the aid of PEI and HAc allowed increasing the graphene concentration without significantly altering its characteristics. The ratios (I_D/I_G) and (I_{2D}/I_G) are equal to 0.74 and 0.44, respectively, for D2, while for mG the values were 0.69 and 0.41 [24], reinforcing that the material did not suffer major changes after redispersion. For mG and D2, the D peak is at 1346 cm^{-1}. The G peak, on the other hand, presents a displacement of 4 cm^{-1} from mG_NMP to D2, from 1579 cm^{-1} to 1583 cm^{-1}. Finally, the 2D band shifts from 2686 cm^{-1} to 2700 cm^{-1} from mG to D2. It is important to note that here the 2D is a broad band and the mentioned value corresponds to its peak. The spectrum of mG_NMP can be seen in Figure 1, allowing comparison with the spectrum of graphene redispersed in D2.

The DP spectrum (Figure 1) is typical of this material [28] and, as it represents ≤ 2.1 wt% in the films (Table 1), it has little or no influence on the spectra of D2, D3 and D4.

The DP spectrum (Figure 1) has an usual appearance for the PEDOT:PSS blend, according to the literature [7,29-31]. The only PSS visible band is located at 1070-1170 cm^{-1} and is due to the presence of sulfonic acid and sulfonate groups [29,32], and caused by a complex deformation mode, with the distribution of potential energy associated with the stretching of the C-S+C-C+SO_3 bond that presents increased downshift as the ionization degree rises [33]. The absorption bands of PEDOT are intense and here they are labeled as PEDOT-1 to PEDOT-5 to facilitate their identification. The PEDOT-1 peak (1246 cm^{-1}) is caused by the inter-ring stretching of Cα–Cα'; PEDOT-2 (1367 cm^{-1}), to the stretching of the Cβ–Cβ bond; PEDOT-3 (1429 cm^{-1}), to the vibration of Cα=Cβ symmetrical, while Cα=Cβ asymmetrical is responsible for PEDOT-4 (1502 cm^{-1}) [31]; finally, PEDOT-5 (1555 cm^{-1}), originates from the antisymmetric stretching of C=C [32,34] on the thiophene rings at the end and in the middle of the PEDOT chains [35]. It is noteworthy that the addition of DMSO to PEDOT:PSS causes changes in the spectrum in relation to pristine PEDOT:PSS, such as a decrease in the intensity of the PEDOT bands [31] and displacement and narrowing of the most intense peak [7], suggesting a change in the conformation of the chains that leads to better conductivity.

When comparing the DP spectrum with the D3 and D4 spectra (Figure 1), which received the addition of mG, the difference is visible. In region 1 (1200 cm^{-1} to 1400 cm^{-1}) of both spectra, it is noticed that the PEDOT-1 and PEDOT-2 peaks are closer and that the PEDOT-2 peak is more separated from PEDOT-3, due to the contribution of the D peak from D2. Furthermore, the most intense PEDOT-3 peak (region 2, 1400 cm^{-1} to 1500 cm^{-1}) is upshifted (1441 cm^{-1} for D3 and 1437 cm^{-1} for D4) and with a lower intensity. Finally, in region 3 (1500 cm^{-1} to 1600 cm^{-1}), PEDOT-5 became more intense than PEDOT-4, due to the G peak from D2. In the D3 spectrum, at 2700 cm^{-1}, it is possible to see a small bump, due to the 2D peak from D2. It is important to remember that D3 has almost 5 times more graphene than D4. The intensity of the 2D peak in D3 surpasses by far that in D4 (Figure 1b).

The changes in the D3 and D4 spectra compared to the DP spectrum point to the formation of the composite between graphene and PEDOT:PSS, helped by π-π interactions between the aromatic structures of these materials [36,37], as well as possible changes in the PEDOT:PSS chain conformation, promoting more intermolecular π-π interaction that changes the electrical properties of the films [37].

3.2. Sheet Resistance and transmittance

The dispersions containing only mG form films that present emptiness among the particles, so, although graphene has high electrical conductivity,

Table 3. Physical characteristics of the films.

Film type ID	Dispersion	Number of layers	Appearance	%T[a]	SR[b] (kΩ/□)	σ[c] (S/m)
1	D1	1	Non-uniform	77.67 ±0.08	15290 ± 20860	2.18
2.1	D2	1	Relatively uniform	85.52 ±1.32	188260 ± 162840	6.42
2.2	D2	3	uniform	67.51 ±0.48	177880 ± 48840	0.19
3	D3	1	Non-uniform	81.43 ±0.03	2.34 ± 2.70	14245.01
4	D3	1	uniform	87.20 ±2.26	1.46 ± 0.37	22831.05
5.1	D4	1	uniform	93.47 ±0.01	1.07 ± 0.08	31152.65
5.2	D4	3	Non-uniform	88.71 ±1.93	0.41 ± 0.10	20325.20
6	D4	2	Non-uniform	64.60 ±3.55	0.25 ± 0.27	47058.82
7	DP	1	Non-uniform	53.73 ±0.20	1.30 ± 0.41	7692.31
8	DP*	1	Non-uniform	73.20 ±0.04	0.90 ± 0.21	11111.11

[a] refers to the film transmittance at 550 nm; [b] the sheet resistance; and [c] the mean conductivity.

the charge flow suffers discontinuity in these void regions, thus higher local voltage might be required to enable charges' jumping to neighboring particles. In composites, PEDOT/PSS works as a semiconductor matrix, facilitating charge transport. Increasing the number of layers also favors the particle packing, assists the lateral π-π interactions and the charges' hopping between the stacked layers.

Sheet resistance and transmittance results are summarized in Table 3. DP-derived films show sheet resistance values in the range of 900 Ω/□ – 1.3 kΩ/□. The D1 film has a high value of sheet resistance, which is explained by the larger amount of insulating PEI. For D2 (films 3.1 and 3.2), the decreased amount of PEI may cause poorer dispersion, generating agglomerates that act as charge traps, thus resulting in higher sheet resistance compared to D1 (sample 1). The films from D1 and D2 resulted in quite high sheet resistances, explained by the emptiness surrounding the particles, which compromises the charge flow.

The PEDOT:PSS/mG composite films 3 - 6 showed a decrease of up to 6 orders of magnitude compared to films 1 – 2 that contain only mG, from ~188 MΩ/□ to ~250Ω/□. Films 5.1, 5.2 and 6, from D4, also show the influence of the number of layers on the sheet resistance. In addition, film 7 was also produced under a lower rotation speed that is likely to lead to thicker films. The lowest value achieved for film 6, 250 Ω/□, comes at the cost of lower transmittance, ~60%, indicating incremented thickness. Films 5.1 and 5.2 and film 6 used the same dispersion and showed comparable sheet resistance, associated with much higher

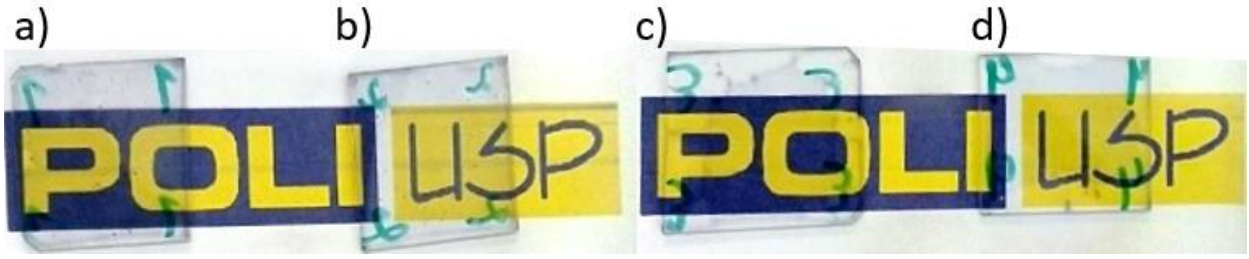

Figure 2. Images of one-layer films prepared by spin-coating, film 4 (a and b) and film 5.1 (c and d).

transmittance values, above 85%, even when more layers were deposited.

Figure 2 shows images of some films 4 and 5.1 that show good reproducibility in the preparation, and exemplify the high transmittance shown in Table 3.

The composite films presented lower resistances compared to those from PEDOT:PSS only, moreover the improvement is still significant, with sheet resistance halving after the addition of mG. Film 7 obtained from DP present several dark spots, discontinuities, and partial coating of the glass. This poor visual uniformity is reinforced by the transmittance results, lower than those found in all other films.

The addition of HAc in IPA to PEDOT:PSS (film 8) slightly improved the uniformity and conductivity of the films, affecting positively its performance. Treatment of PEDOT:PSS films with strong acids is a known technique to improve their conductivity, but it involves washing the films with the acid, not adding them to the dispersion. Liu et al. [4] used acetic acid in isopropanol in mass concentrations between 40% and 100% to treat PEDOT:PSS films, obtaining results of sheet resistance of 0.213 kΩ/□ for 80% HAc in IPA [4]. Besides, the addition of IPA to PEDOT:PSS promotes wettability and increases the adhesion of the films to the glass, and 50% of IPA reduced the resistivity slightly, according to Borazan et al. [38] this may also explain the higher transmittance of film 8 in relation to films 7 [38].

It is interesting to compare the results of D3 and D4. Although D3 contains almost 5 times more mG than D4, its sheet resistances are higher, possibly due to the presence of mG clusters in D3 films. Films from both dispersions show high transmittances, although minimum dark spots are seen, indicating both mG agglomeration and presence of polymeric gels due to the large sized polymer chains or a non-homogeneous ionization of the PSS [39]. One way to solve this problem is by centrifuging the PEDOT:PSS, prior to deposition, and remove the poor soluble fraction.

The decrease in sheet resistance in composite films can be explained by the presence of conductive graphene in the semiconducting polymer matrix. Yoshida [39] deposited composite films of PEDOT:PSS and conductive silver ink, associating the decrease in the resistivity of the films with the presence of micrometric silver particles between the polymer chains, aiding the movement of the charge carriers and reducing the energy required for it. It is reasonable to assume that an analogous situation occurs as mG may present segments of dioxythiophene anchored onto its surface, increasing the cohesion of the solid film, provided it is well dispersed. Furthermore, the addition of DMSO alters the conformation of the chains, exposing these dioxythiophene segments by stretching the PEDOT chains, also contributing to the charge mobility [39].

The decrease in the sheet resistance in polymer/graphene composites is attributed to the high conductivity and high electronic mobility of graphene, which acts as a conducting medium for the charges [40-42]. The energy levels' compatibility between PEDOT and graphene contributes to their strong π-π interaction and the electrostatic repulsion between graphene and PSS that supports the formation of homogeneous film [43-46]. According to Kim et al. [45], PEDOT chains are absorbed on the graphene surface, the dioxythiophene groups donate electrons to graphene and increase the concentration of charge carriers, whereas the chains assume a linear or expanded coil conformation. Moreover, due to the intermolecular π-π interactions, the influence of the PEDOT conjugation defects reduces and facilitates charge transfer, decreasing the barrier to their movement. Additionally, the extension of the conjugated π-system increases and the π-π* band gap narrows, resulting in larger number of charge carriers and higher charge carriers' mobility.

However, increasing the concentration of graphene also represents an increase in the concentration of defects, such as voids in the material, so they will not reflect a continuous increase in conductivity, as such defects are charge traps that will influence the charge concentration and mobility [45]. Therefore, large amount of graphene may also cause aggregation and reduce the conductivity of the films, as in the case of D3.

The conductivities of the films (Table 3) was calculated considering that the thickness of the films are 30 nm for 1 layer, 85 nm for 2 layers and 120 nm for 3 layers for the composites, while 80 nm for 3 layers for mG, and 100 nm for 1 layer of DP

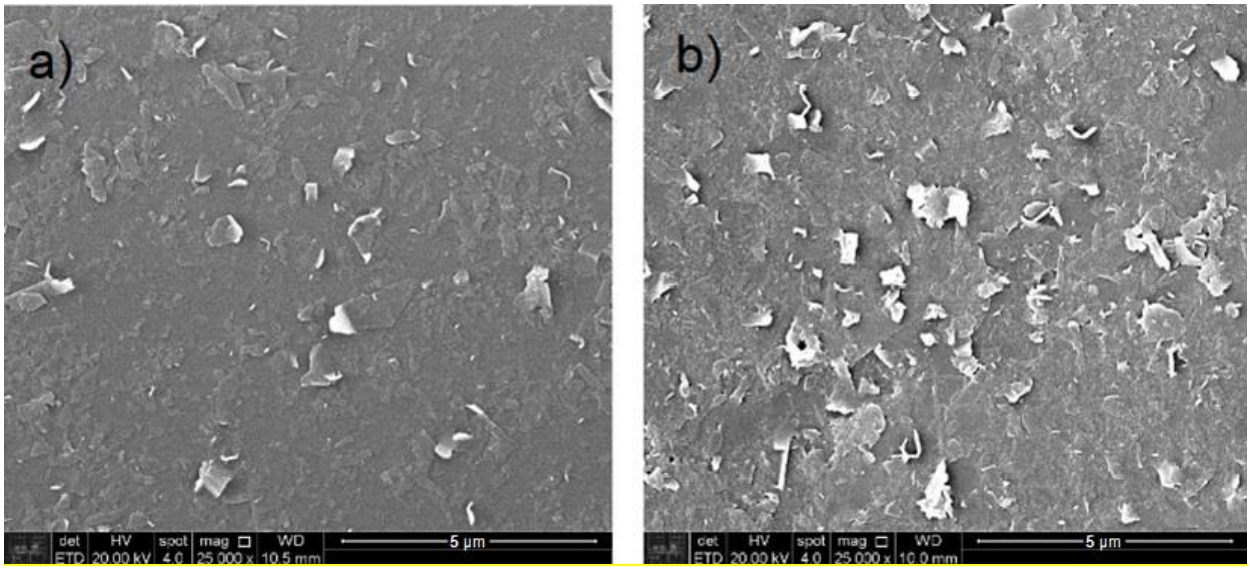

Figure 3. Micrographs with 25000x magnification of the dispersions a) D2 and b) D4.

and DP*. The thicknesses were estimated by AFM, except for DP and DP*, which presented low transmittances. The results indicate that lower values of sheet resistance for thicker films, as expected, is not a rule, in fact, some films present lower conductivity as more layers are deposited, which is exemplified by 2.2 vs. 2.1 or 5.2 vs. 5.1 and 6, demonstrating that for the same composite the inner microstructure (cohesiveness) of the film prevails over the composition regarding the mobility of the charge carriers.

TCEs have several applications, each with its specific requirements. Transmittance values usually vary between 86% and 92% and sheet resistance values can range from 30 Ω/□ to 1500 Ω/□ [47], so the films obtained from D3 and D4 are potential candidates in this kind of application.

The results presented here are comparable to sheet resistance results reported in the literature. Li et al. [48] prepared PEDOT:PSS/graphene composites from an aqueous slurry of graphene and obtained films with transmittances of about 90% and sheet resistances between 1902 Ω/□ and 2980 Ω/□. Uz et al. [49] manufactured graphene films with a sheet resistance of 200 Ω/□, suggesting its use in biomedical applications. Fang and his group [50] manufactured PEDOT:PSS/graphene films by spin and blade coating on PET substrates, with the best results being 80.6% transmittance with a sheet resistance of 731 Ω/□ and 85% of transmittance with a sheet resistance of 1783 Ω/□.

Thus, given their electrical and optical properties, the composites developed in this work can be used as TCEs. Another suggested application for these materials is in conductive trails.

3.3. Scanning electron microscopy

Figure 3 shows two SEM micrographs at 25000x magnification. No significant differences are observed between mG films and mG/ PEDOT:PSS composite films. It is noted in both images, the mG sheets “popping out” of the films, this effect being greater in D4, which seems to present higher roughness. In Figure 3a, it can be seen that mG is extensively well dispersed, but the electrical measurements have shown that there is no effective conductive medium between the sheets, since this sample is from D2, only mG film. Figure 3b shows a D4 composite film, mG dispersed in PEDOT:PSS matrix, in which, apparently, there are conductive paths for the charge carriers (Table 3). The discrete emptiness between the sheets in D2, which is responsible for the low electrical performance, is not observable under SEM. We believe that the composites can be improved by using smaller amounts of mG as additive in order to avoid aggregation that serves as charge traps, a factor that is even more relevant when considering D3, which has 5 times more mG than D4.

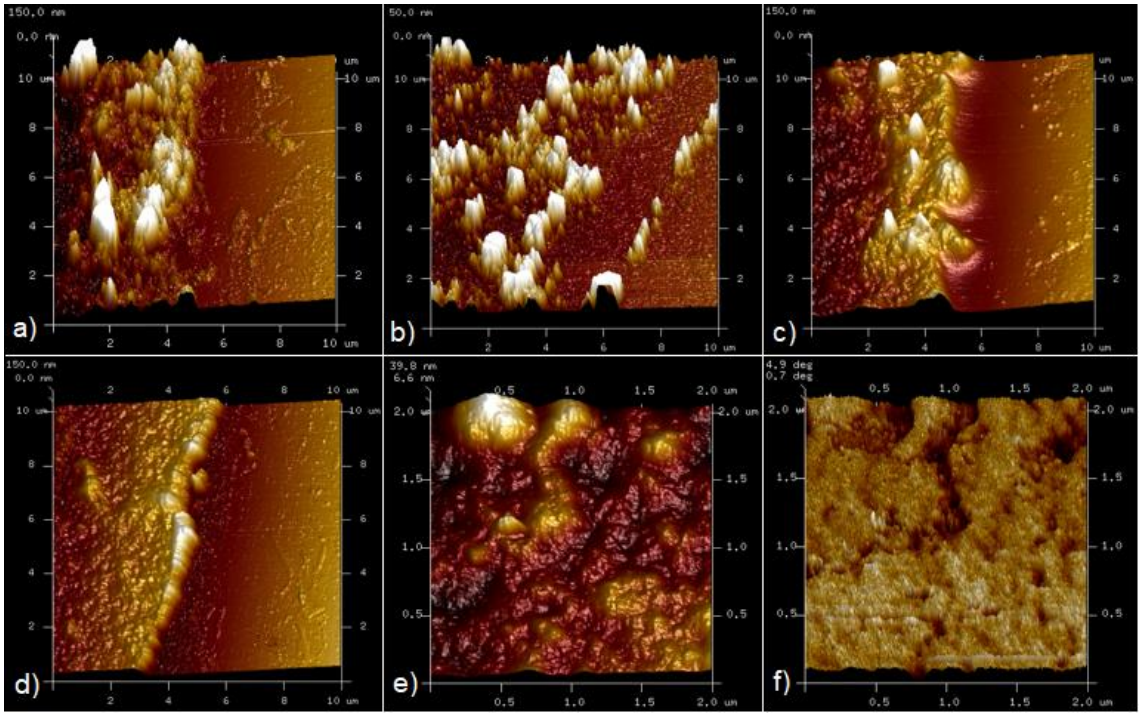

Figure 4. AFM images of films. a) Step region of sample AFM1 (D2, 3-layer, 81 nm); b) Step region of sample AFM2 (D4, 1-layer, 29 nm); c) Step region of sample AFM3 (D3, 2-layer, 85 nm); d) Step region of sample AFM4 (D4, 3-layer, 117 nm); e) Magnification of the surface of sample AFM4; and f) Phase image of sample AFM4.

3.4. Atomic Force Microscopy

Figures 4a - 4d show the step regions in which the film thicknesses were measured. Figure 4a corresponds to the sample AFM1 (D2) with a thickness of 81 nm. Figure 4b corresponds to the AFM2 sample (D4) with a thickness of 29 nm. When comparing this result to the thicknesses values of samples AFM3 (D3) and AFM4 (D4) (Figures 4c and 4d, respectively), we observed that the deposition of a new layer of composite film onto an existing layer, in fact, does not contribute equally to the thickness, reaching 85 nm and 117 nm, respectively. Note that the samples AFM1 and AFM4 have the same number of layers, but the first is consisted of mG only, not PEDOT:PSS/mG. It should not be forgotten that the variations in the images are on the order of nanometers, so the films can be considered homogeneous. Furthermore, adding more layers seems to make the films more compact and uniform.

Figure 4e shows another morphological image of the AFM4 sample, away from the step and with higher magnification, where it is possible to notice uniformity of the film, once again. A phase image (Figure 4f) is collected from the same area, which allows us to draw some conclusions about the film. Phase images of PEDOT:PSS films present light regions associated to the PEDOT-rich regions (more rigid) and dark regions, to the PSS-rich regions (softer) [29,30,34,35,51,53]. On the other hand, in graphene/PEDOT:PSS composite films [29,34], the third component is not easily discernible, however the occurrence of an uniform phase image may indicate film densification, which increases conductivity [53]. Thus, the AFM results help to explain the sheet resistance results, indicating that the performance is linked to the extension and the interconnectivity of the graphene-rich (lighter) and PEDOT-rich (lighter) regions, which form the conductive medium. The dark regions are likely to be non-conducting PSS-rich regions. Therefore, once the existing dark regions do not interfere with the continuousness of the light regions, decrease of the resistance is favored.

4. CONCLUSIONS

In this work, the production and characterization of PEDOT:PSS/mG composites were demonstrated.

The transmittance and sheet resistance results qualify the materials presented here to be used as TCEs, in applications such as OLEDs and OPVs.

Raman spectroscopy showed that the redispersion with the aid of HAc and PEI in IPA incremented the mG concentration reaching 10 mg/mL in IPA, without significant changes in the Raman spectrum of the films, indicating that no significant defects were introduced and that there were no agglomeration of the nanomaterial. In addition, the composites presented the bands observed in the mG spectrum.

Sheet resistances of the composite films decreased by 6 orders of magnitude from those of mG films only, while they are just ca. one half of those found for the PEDOT:PSS films. The properties were correlated to the composition and structure of the materials, raising the hypothesis that the strong π-π interactions between graphene and PEDOT and the transfer of electrons from PEDOT to graphene contribute to the cohesiveness of the film and increases the number of charge carriers and mobility, therefore the composite present higher conductivity.

The thicknesses of the films were estimated by AFM, and the results have shown that depositing additional layers makes the films more compact and uniform, which is also beneficial for reducing the resistance. Furthermore, the phase image compared to the morphological image shows that there are soft regions, corresponding to the PSS-rich domains, and more rigid regions, comprised mainly by PEDOT and mG, showing once again the formation of a composite having interconnected conductive domains.

ACKNOWLEDGMENTS

We thank the Brazilian Coordination for the Improvement of Higher Education Personnel (CAPES, finance code 001) and the Brazilian Council for Scientific and Technological Development (CNPq 306212/2018-8) for financial support and the Nacional de Grafite LTDA (Brazil) for donation of the pristine graphite (99.6%). We also thank M.Sc. Igor Yamamoto Abê for the assistance to acquire Raman spectra, Dr. Daniel Luiz Rodrigues Júnior for the SEM images. We are grateful to the “Laboratório de Filmes Finos do Instituto de Física da Universidade de São Paulo”, Brazil, for AFM images.

REFERENCES

[1] H. Jang; MS Kim; W. Jang; H. Son and DH Wang, *J. of Industrial and Engineering Chemistry*, **86**, 205 (2020).
[2] R. Fischer; A. Gregori; S. Sahalkalkan; D. Hartmann; P. Büchele; SF Tedde and O. Schmidt, *Organic Electronics* **62**, 351 (2018).
[3] AK Sarker; J. Kim; B.-H. Wee; H.-J. Song; Y. Lee; J.-D. Hong and C. Lee, *RSC Adv.* **5**, 52019 (2015).
[4] G. Liu; Y. Liu; M. Zhang; Z. Yang and P. Gane, *Organic Electronics* **81,** p. 105674. (2020).
[5] J. Saghaei; F. Ali and T, Saghaei, *Organic Electronics* **24**, 188 (2015).
[6] F. Zabihi; Y.Xie; S. Gao and M. Eslamian, *Applied Surface Science* **338**, 163 (2015).
[7] J. Ouyang, *Displays*, **34**, 423 (2013).
[8] C.-K. Cho; W.-J. Hwang; K. Eun; S.-H. Choa; S.-I. Na and H.-K. Kim, *Solar Energy Materials & Solar Cells*, **95**, 3269. (2011).
[9] J. Gasiorowski; R. Menon; K. Hingeri; M. Dachev and NS Sariciftci, *Thin Solid Films*, **536**, 211 (2013).
[10] SH Chang; W.-N. Chen; C.-C. Chen; S.-C. Yeh; H.-M. Cheng; Z.-L. Tseng; L.-C. Chen; KY Chiu; W.-T. Wu; C.-T. Chen, S.-H. Chen, and C.-G. Wu, *Solar Energy Materials & Solar Cells*, **161**, 7 (2017).
[11] CS Pathak; JP Singh and R. Singh, *Chemichal Physics Lett.* **694**, 75 (2018).
[12] NA Sarkhan; ZA Rahman; A. Zakaria and AMM Ali, Materials Today: Proceedings, **17**, 484 (2019).
[13] DP Kepić; ZM Markovic; SP Jovanović; DV Peruško; MD Budimir; HDI Antunović; VB Pavlović, BMT Marković, *Synthetic Metals* **198**, 150 (2014).
[14] MJ Allen, VC Tung and RB Kaner, *Chem. Rev.*, **110**, 132. (2010).
[15] AK Geim and KS Novoselov, *Nature Materials*, **6**, 183. (2007).
[16] AH Neto; F. Guinea; NMR Peres; KS Novoselov; and AK Geim, *Reviews of modern physics* **81**, 109. (2009).
[17] F. Bonaccorso; Z. Sun.; T. Hasan and AC Ferrari, *Nature Photonics* **4**, 611 (2010).
[18] M. Lotya; PJ King; U. Khan; S. De and JN Coleman, *ACS Nano* **4**, 3155 (2010).
[19] X. You; Q. Feng; J. Yang; K. Huang; J. Hu; S. Dong, *J. Nanopart. Res.* **21**, 19 (2019).
[20] W. Hong; Y. Xu; G. Lu; C. Li and G. Shi, *Electrochemistry Communications*, **10**, 1555 (2008).
[21] M. Hilal and JI Han, *Synthetic Metals* **245**, 276 (2018).
[22] C. Park; D. Yoo; S. Im; S. Kim; W.Cho; J. Ryu and JH Kim, *RSC Adv.* **7**, 25237 (2017).
[23] J. Santos, *Preparation of graphene through liquid phase exfoliation and nanocomposite semiconductor thin films*, Depto. Eng. Metal. Materials, Polytechnic School, University of São Paulo, São Paulo (2019)
[24] R. Matroniani; FT Mabilia; JS Santos and SH Wang, Journal of the Brazilian Chemichal Society, submitted in 2022, (2022)
[25] C. Casiraghi; A. Hartschuh; H. Qian; S. Piscanec; C. Georgi; A. Fasoli; KS Novoselov; DM Basko; AC Ferrari; *Nano Lett.* **9**, 1433 (2009).
[26] LG Cançado; A. Jorio; EHM Ferreira; F. Stavale; CA Achete; RB Capable; MVO Moutinho; A. Lombardo; TS Kulmala; AC Ferrari; *Nano Lett.* **11**, 3190 (2011).
[27] AK Singh; V. Chaudhary; AK Singh; SRP Sinha; *RSC Advances.* **11**, 3096 (2021).
[28] S. Sanchez-Cortes; RM Berenuel; A. Madejon and M. Pérez-Mendez, *Biomacromolecules* **3**, 655 (2002).
[29] Y. Seekaew; S. Lokavee; D. Phokharatkul; A. Wisitsoraat; T. Kerdcharoen and C. Wongchoosuk, *Organic Electronics* **15**, 2971 (2014).
[30] PG Raj; VS Rani; A. Kanwat and J. Jang, *Materials Research Bulletin* **74**, 346 (2016).

[31] SH Chang; C.-H. Chiang; F.-S. Kao; CL. Tien and CG. Wu, *IEEE Photonics Journal* **6**, 8400307 (2014).
[32] AA Farah; SA Rutledge; A. Schaarschmidt; R. Lai; JP Freedman and AS Helmy, *Journal of Applied Physics* **12**, 113709 (2012).
[33] JM Alia; HGM Edwards and BM Kiernan, *Spectrochimica Acta Part A* **60**, 1533, (2004).
[34] B. Huang; X. Luo; Q. Zou; S. Wang and d J. Zhang, *RSC Adv.* **9**, 42335 (2019).
[35] D. Jucius; A. Lazauskas; V. Grigaliunas; A. Guobiene; I. Prosicevas; B. Abakeviciene and M. Andrulevicius, *Materials Research* **22**, e20190134 (2019).
[36] D. Yoo; J. Kim and JH Kim, *Nano Research* **7**, 717 (2014).
[37] B. Brennan; SJ Spencer; NA Belsey; T. Faris; H. Cronin; SRP Silva; IS Gilmore; Z. Stoeva and AJ Pollard, *Applied Surface Science* **403**, 403 (2017).
[38] I. Borazan; AC Bedeloglu and A. Demir, *Polymers and Polymer Composites* **28** (1), 66 (2020).
[39] S. Yoshida *"PEDOT:PSS-based polymeric systems for application as device circuits and electrodes "* , Dept. Eng. Metal. Materials, Polytechnic School of the University of São Paulo, São Paulo (2015)
[40] H. Chang; G. Wang; A. Yang; X. Tao; X. Liu; Y. Shen and Z. Zheng, *Adv. Function Mater.* **20**, 2893 (2010).
[41] F. Soltani-kordshuli; F. Zabihi and M. Eslamian, *Engineering Science and Technology, an International Journal* **19**, 1216 (2016).
[42] S. Khasim; A. Pasha; N. Badi; M. Lakshmi and YK Mishra, *RSC Adv.* **10**, 10526 (2020).
[43] M. Zhang and JTW Yeow, *Carbon* **156**, 339 (2020).
[44] L. Wan; B. Wang; S. Wang; X. Wang; Z. Guo; B. Dong; L. Zhao; J.Li; Q. Zhang and T. Luo; *J. Mater. Sci.* **50**, 2148 (2015).
[45] GH Kim; DH Hwang and SI Woo, *Phys. Chem. Chem. Phys*, **14**, 3530 (2012).
[46] C. Redondo-Obispo; TS Ripolles; S. Cortijo-Campos; AL Alvarez; E. Climent-Pascual; A. de Andrés and C. Coya, *Materials and Design* **191**, 108587 (2020).
[47] DS Hecht; L. Hu and G. Irvin, *Adv. Mater.* **23**, 1482 (2011).
[48] Z. Li; X. Zhang; L. Shen; Z. Fan; X. Chen; M. Chen; S. Qiu; F. Zabihi; M. Eslamian and Q. Chen; *J. Coat. Technol. Res.* **16** (6), 1773 (2019).
[49] M. Uz; K. Jackson; MS Donta; J. Jung; MT Lentner; JA Hondred; JC Claussen and SK Mallapragada, *Scientific Reports* **9**, 10595 (2019).
[50] X. Fang; Z. Fan; Y. Gu; J. Shi; M. Chen; X. Chen; S. Qiu; F. Zabihi; M. Eslamian and Q. Chen, *J. Shanghai Jiao Tong Univ. (Sci.)* **23** (1), 106 (2018).
[51] HS Dehsari; EK Shalamzari; JN Gavgani; FA Taromi and S. Ghanbary, *RSC Adv.* **4**, 55067 (2014).
[52] A. Hasani; HS Dehsari; JN Gavgani; EK Shalamzari; A. Salehi; FA Taromi and M. Mahyari, *Microchim Acta* **182**, 1551 (2015).
[53] X. Wang; AKK Kyaw; C. Yin; F. Wang; Q. Zhu; T. Tang; PI Yee and J. Xu, *RSC Adv*. **8**, 18334 (2018).